J. Plasma Fusion Res. SERIES, Vol. 4 (2001) 146–152

Electric Potential Cells at the Diverted Tokamak Separatrix

SCHAFFER Michael J.*, PORTER Gary D.[1], BOEDO Jose A.[2], BRAY Bruce D.,
HSIEH Chung-Lih, MOYER Richard A.[2], ROGNLIEN Thomas D.[1],
STANGEBY Peter C.[3] and WATKINS Jonathan G.[4]
General Atomics, P.O. Box 85608, San Diego, California 92186-5608, USA
[1]*Lawrence Livermore National Laboratory, Livermore, California 94551, USA*
[2]*University of California, San Diego, California 92093-0417, USA*
[3]*University of Toronto, Toronto, ON M3H 5T6, Canada*
[4]*Sandia National Laboratories, Albuquerque, New Mexico, USA*

(Received: 5 December 2000 / Accepted: 18 August 2001)

Abstract

Two-dimensional measurements by probes and Thomson scattering reveal unanticipated electric potential and electron pressure (p_e) maxima near the divertor X-point in L-mode plasmas in the DIII-D tokamak. The potential hill (~100 V) drives $\boldsymbol{E}\times\boldsymbol{B}$ circulation ("potential cell") of particles, energy and toroidal momentum around the X-point and in and out across the magnetic separatrix. Modeling by the UEDGE two-dimensional edge transport code with plasma drifts shows similar X-point potential and pressure hills. The code predicts additional drift-driven nonuniformity poloidally around the separatrix. Potential cells in UEDGE arise from parallel (to $\boldsymbol{B}$) viscous stress acting on the Pfirsch-Schlüter ion return flow of the ∇B drift. These experimental and theoretical results demonstrate that the boundary layer just inside the separatrix of low power tokamak plasmas can be far from poloidal uniformity. We speculate that separatrix potential cells might be a major feature of L-mode edge transport and their suppression an important feature of H-mode.

Keywords:

electric potential, electric field, $\boldsymbol{E}\times\boldsymbol{B}$ drift, plasma flow, plasma viscosity, X-point, divertor, divertor X-point

1. Introduction

Many tokamaks divert exhaust plasma along magnetic lines to target surfaces somewhat removed from the main plasma. The magnetic separatrix, indicated in Fig. 1, separates the interior region of plasma, confined on closed toroidal magnetic surfaces, from the open line scrape-off layer (SOL), where plasma flows almost parallel to the magnetic field $\boldsymbol{B}$ to targets, where it deposits its energy and recombines. The X-point, a poloidal magnetic field null, defines the separatrix in conventionally diverted tokamaks. The region between the separatrix-target strike points is called the private region, because its magnetic lines do not encircle the confined plasma. It is beneath the X-point in Fig. 1. The region roughly from the X-point to the targets is usually called "the divertor."

The X-point is the apex of four quadrant regions: the private region, the inner and outer SOLs (at major radius R smaller and larger than the X-point, respectively) and closed confinement surfaces. The X-point region is complex, because the four plasma quadrants, each with distinct temperature, density and electric potential, meet there. Theoretical analysis predicts the

*Corresponding author's e-mail: schaffer@fusion.gat.com

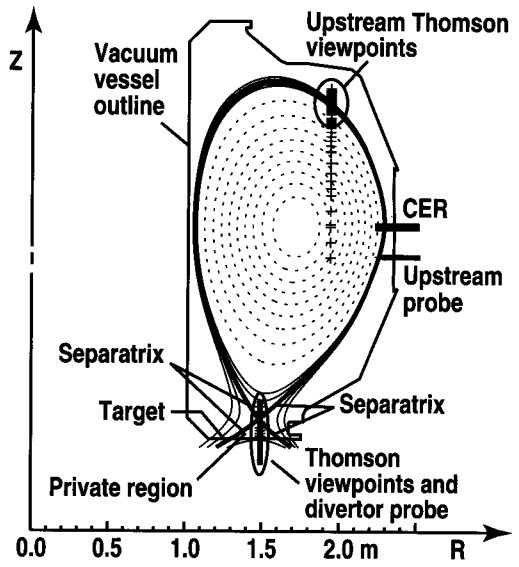

Fig. 1 Single-null diverted plasma geometry inside the DIII-D vacuum vessel outline, with the disposition of probe, Thomson scattering and CER diagnostics. The 98% and 99% ψ_n surfaces are drawn inside the separatrix and the 101% and 102% surfaces outside.

formation of a boundary layer across the separatrix to accommodate the disparate regions [1]. Numerical solutions of the edge plasma by the UEDGE computer code [2,3] with electric potentials and magnetic gradient drifts self consistently included [4-6] indeed exhibit a boundary layer just inside the separatrix. These solutions also demonstrated the existence and importance of a large $\boldsymbol{E}\times\boldsymbol{B}$ plasma convection in the private region [4]. Recent measurements of the electric potential [7] in the divertor of the DIII-D tokamak [8] confirmed the private $\boldsymbol{E}\times\boldsymbol{B}$ convection in quantitative agreement with the Ref. [4] prediction. Further measurements revealed unexpected local electric potential and electron pressure (p_e) maxima near the X-point in DIII-D L-mode (low confinement) plasmas [9,10]. The potential hill (~100 V) drives $\boldsymbol{E}\times\boldsymbol{B}$ circulation ("potential cell") of particles, energy and toroidal momentum around the X-point and in and out across the magnetic separatrix. New UEDGE modeling at lower power and confinement than in Refs. [4-6] develops similar X-point potential cells and further predicts additional drift-driven poloidal nonuniformity around the separatrix [10]. The present paper reports the experimental and numerical potential cells near the separatrix and explains them as a consequence of parallel ion viscous stress acting on the Pfirsch-Schlüter ion return flow of the ∇B drift.

2. Experimental Results

The experiments were performed in the DIII-D tokamak [8]. The plasma was diverted by a single magnetic null to the lower target. Figure 1 shows a typical geometry. The divertor plasma was attached to the target at the outer strike point and detached at the inner, which is typical in DIII-D.

The plasma electric potential Φ was measured by a pair of fast-stroking Langmuir probe arrays, one moving vertically through the divertor region [11] and the other horizontally through the upstream SOL just below the torus equatorial plane [12]. The probe stroke paths are indicated in Fig.1. Two Thomson scattering systems provided the primary measurements of T_e and electron density n_e. The divertor Thomson scattering system [13] measured at eight vertically separated locations at the same radius as the divertor probe, as shown in Fig. 1. The upstream Thomson scattering system [14] measured at many closely spaced points ($\approx$ 13 mm separation) vertically across the edge and SOL, as shown in Fig. 1. Plasma ion temperature T_i was measured near the equator by charge exchange recombination spectroscopy (CER) [15]. No suitable T_i diagnostic covers the X-point in DIII-D. To obtain data in two dimensions, the X-point was magnetically scanned radially past the divertor diagnostics, between the extremes as shown in Fig. 2. The X-point was positioned about 0.13 m above the target, closer than usual, to provide good diagnostic coverage above the X-point. Magnetic surfaces were calculated by the equilibrium fitting code EFIT [16]. They are labeled by their normalized poloidal magnetic flux, ψ_n. $\psi_n = 1$ is the separatrix, $\psi_n > 1$ is the SOL with ψ_n increasing outward from the separatrix, and $\psi_n < 1$ is in either the closed confinement or open private region with ψ_n decreasing inward from the separatrix. Additional information about the measurements is contained in Refs. [9,10].

We present data from low power L-mode plasmas, which display the most interesting X-point behavior. The applied toroidal magnetic field was B_T = 2.0–2.1 T at radius R = 1.7 m; plasma current was I_p = 1.0 MA; line average electron density was 2.5×10^{19} m^{-3}; and heating was 0.6 MW Ohmic and 0.3 MW neutral beam power. Both B_T directions were employed. The plotted data are from discharges with B_T directed out of the page in Fig. 1 ("standard" B_T, ion ∇B drift toward the X-point). The X-region profiles for "reversed" B_T (ion ∇B drift away from the X-point) are not markedly different.

Figure 3 shows the plasma potential distribution in

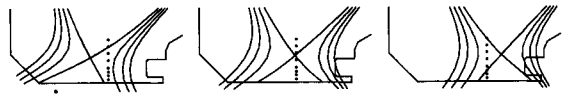

Fig. 2 Range of divertor geometry used to measure around the X-point.

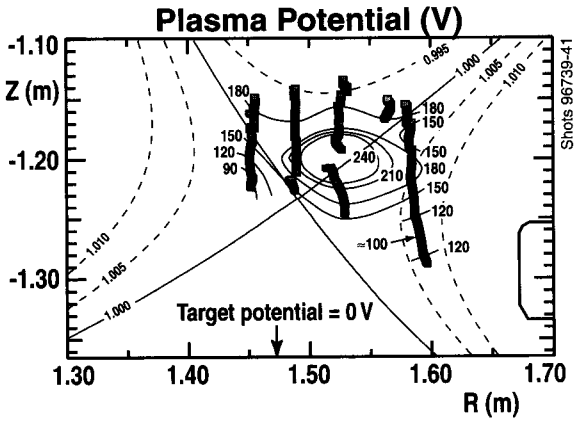

Fig. 3 Plasma potential for ion ∇B drift toward the X-point. Small squares indicate measurements. Outer midplane potential is ≈ 50 V with almost no radial variation across the magnetic surfaces shown.

the divertor and X-region. The potential in the three quadrants with data is positive (100–250 V) and much larger than the upstream potential (~50 V) on the same magnetic surface. Therefore, Φ is high (potential hill) by as much as 200 V near the X-point. The potential was roughly similarly distributed in shots with reversed B_T, but it was lower, ~100 V in the X-region and ~25 V upstream. We conclude that a positive potential hill exists near the X-point on SOL, closed and private surfaces, in L-mode plasmas for both B_T directions. The large potential difference between the X and upstream locations on closed surfaces is remarkable, because neoclassical plasma theory predicts only a weak poloidal potential variation, $e\Delta\Phi \ll kT_e$. In the SOL, the non-monotonic poloidal potential variation, from target (Φ = 0) to potential hill in the X-region to a lower value upstream, is also noteworthy, because it is commonly expected that Φ should increase monotonically with T_e (T_e ~5 eV at target, ~50 eV upstream).

Figure 4 shows electron pressure, $p_e = n_e T_e$, from Thomson scattering from a shot in the same series as Fig. 3. The data show that p_e near the X-point (100–150 Pa) is about 2–3 times greater than upstream on magnetic surfaces near the separatrix (≈ 50 Pa). Therefore, there is also a p_e maximum or hill near the X-point. The p_e hill is associated with a corresponding greater n_e near the X-point relative to upstream. The p_e hill is observed in L-mode with both B_T directions and in the few Ohmically heated plasmas for which we have data. The X-point non-uniformity extends inward for about 1% of poloidal flux from the separatrix. In contrast, p_e in H-mode appears to be uniform on the closed surfaces [10].

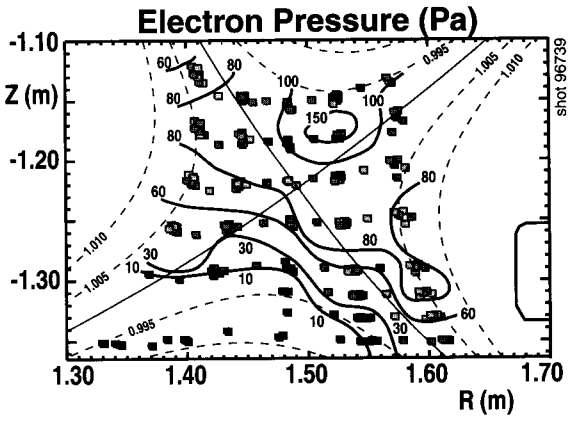

Fig. 4 Electron pressure for ion ∇B drift toward the X-point. Small squares indicate measurements. Upstream p_e are 60 Pa, 40 Pa, and 30 Pa at ψ_n = 0.995, 1.000 and 1.005, respectively.

3. X-point Potential Cell

The experimental near-separatrix plasmas are sufficiently collisional to justify use the Braginskii MHD plasma equations [17]. The potential gradient on a magnetic surface is governed by a balance of the parallel forces acting on electrons, which in the low resistivity collisional limit is

$$e\nabla_{\|}\Phi = -eE_{\|} \approx \nabla_{\|} p_e/n_e + 0.71\nabla_{\|} kT_e \,. \qquad (1)$$

The last term is the parallel thermal force. On closed magnetic surfaces just inside the separatrix and on open SOL surfaces at or upstream of the X-point, T_e has very little parallel gradient, so $e\nabla_{\|}\Phi \approx kT_e\nabla_{\|}\ln(n_e)$, and the locally high potential is associated with locally high electron density. However, T_e decreases toward the targets, and the full equation must be used downstream. In general, a p_e hill at the X-point implies an associated potential hill and can be used as a proxy for it. This is convenient, because direct potential measurement by Langmuir probes is difficult as plasma heating power is increased. In fact, an X-point p_e hill is measured by Thomson scattering in high-power L-mode plasmas, but

not in H-mode [10]. If Eq. (1) is evaluated just inside the separatrix, where $T_e \approx 50$ eV, and the X-point and upstream densities are 1.5×10^{19} m^{-3} and 0.6×10^{19} m^{-3}, respectively, it yields an X-point potential only 46 V more positive than upstream. This is much less than the ~200 V measured. The potential data are very noisy and perhaps are not accurate. The agreement between Eq. (1) and data for reversed BT is better.

The origin of the near-X p_e hill relative to upstream p_e must be explained. We proposed a mechanism based on constancy of total pressure, $p = p_e + p_i$, between the X-region and upstream, combined with strong ion cooling in the divertor [9,10]. This model is plausible for low power L-mode plasmas like the ones in Figs. 3 and 4, but not for high-power L-mode. New modeling by the UEDGE edge transport code, presented in the next Section, suggests that parallel ion viscosity plays a major and more general role in generating potential cells near the separatrix.

The cross-$\boldsymbol{B}$ potential gradient drives plasma along equipotentials around the X-point at the electric drift velocity, $\boldsymbol{v}_E = \boldsymbol{E}\times\boldsymbol{B}/B^2 \approx -\nabla\Phi \times \boldsymbol{B}_T/B_T^2$. We use the tokamak approximation, $B \approx B_T$. Although the potential distribution cannot be measured over the full edge plasma volume with the available DIII-D diagnostics, the X-point potential hill must contribute an $\boldsymbol{E}\times\boldsymbol{B}$ circulation qualitatively like the one sketched in Fig. 5. It convects particles, energy and momentum out and in across the separatrix. The divertor drift, especially the drift across the private region, has been discussed theoretically [4,5] and observed experimentally [7]. The private drift was shown to be the main factor causing the long-observed sensitivity of the inner-outer divertor target plasma differences to the B_T direction [4,5]. The potential hill observed on closed surfaces near the X-point, reported above, extends that circulation into the confinement volume.

The $\boldsymbol{E}\times\boldsymbol{B}$ exchange time, defined as the time for a fluid element traveling at $\boldsymbol{v}_E$ to go from an entry to an exit point on an equipotential surface, is $\tau_{ex} \approx |B\ dA/d\Phi|$. Here dA is the area in the R-Z plane enclosed between equipotential surfaces Φ and $\Phi + d\Phi$ in the volume of interest. For the potential hill region above the X-point, roughly the area bounded by the separatrix, the $\psi_n = 0.99$ surface and extending part way upstream, $A \sim 0.01$ m^2. Approximating $dA/d\Phi$ by $A/|\Phi_2 - \Phi_1|$, with $|\Phi_2 - \Phi_1| = 65$ V, yields $\tau_{ex} \sim 0.3$ ms. It is noteworthy that τ_{ex} is much shorter than the ion-neutral charge exchange time, which is $\gtrsim 3$ ms for neutral density measured at $\lesssim 1\cdot10^{16}$ m^{-3} in the X-region of similar discharges in the same experimental series [18]. X-region charge exchange has been advanced as significant mechanism to remove plasma angular momentum and perhaps influence the tokamak H-mode [19,20]. However, the X-region $\boldsymbol{E}\times\boldsymbol{B}$ circulation is much greater. For $\tau_{ex} = 0.3$ ms, the rate of $\boldsymbol{E}\times\boldsymbol{B}$ angular momentum circulation across the separatrix is ≈ 0.14 N·m, which is comparable with ≈ 0.16 N·m injected by the neutral beam. Similarly, the $\boldsymbol{E}\times\boldsymbol{B}$ circulation of ions out across the separatrix is large, $\approx 3\cdot10^{21}$ s^{-1}, more than half of the total cross-separatrix transport rate ~ $5\cdot10^{21}$ s^{-1}. Clearly, the X-point potential cell plays a significant and previously unappreciated role in transport across the separatrix.

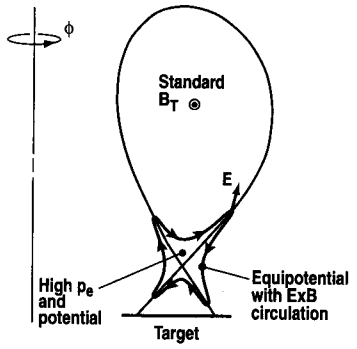

Fig. 5 Qualitative $\boldsymbol{E}\times\boldsymbol{B}$ circulation around the X-point.

4. Numerical Modeling

The two-dimensional multi-species edge transport code UEDGE [2,3] was previously used to model a generic, single-null-diverted, DIII-D H-mode discharge with self-consistent inclusion of $\boldsymbol{E}\times\boldsymbol{B}$ and ∇B drifts [4-6]. Recent numerical improvements to the code have facilitated its use to model other plasmas with the drifts. Here we show new results from modeling a low-power (0.7 MW radial power flow), single-null-diverted DIII-D L-mode plasma. A constant impurity (carbon) fraction was used here. UEDGE obtains $T_e \approx 50$ eV, just inside the separatrix, like the experiment, and it is nearly uniform poloidally. The model plasma differs from the experimental ones reported above mainly in its divertor geometry, which has about twice the divertor leg length of the experiments. The UEDGE inner divertor plasma is detached from its target, as in the experiment.

Figures 6 and 7 show, respectively, the UEDGE-calculated potential and p_e distributions in the divertor and X-region for standard B_T direction. The p_e distribution is close to the experimental one in Fig. 4.

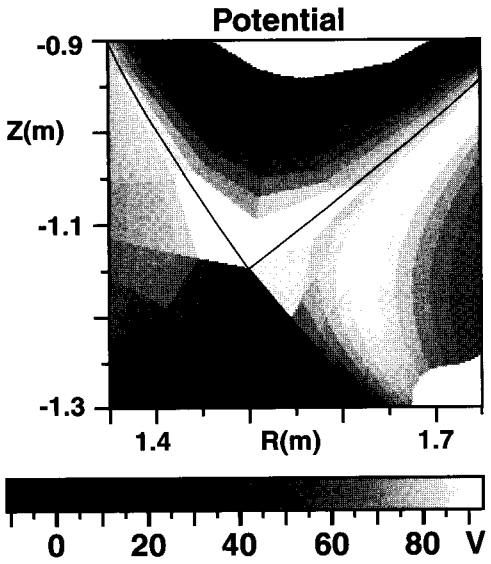

Fig. 6 UEDGE-calculated Φ distribution.

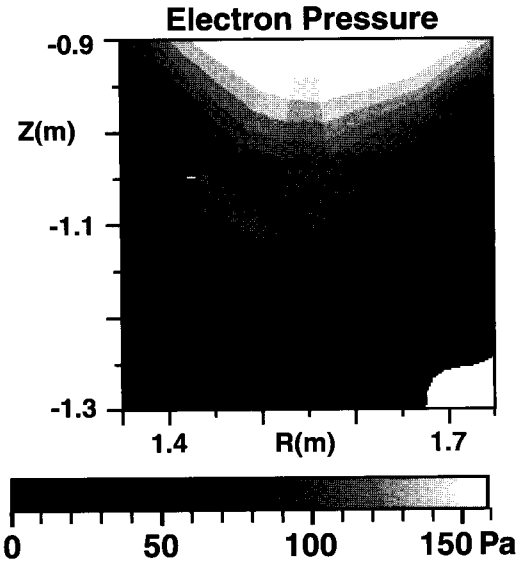

Fig. 7 UEDGE-calculated p_e distribution.

However, the UEDGE potential is considerably smaller in magnitude than the experimental one in Fig. 3. This might arise in part from the different divertor geometry, but, as noted in Section **3**, it is also likely that the measured potentials have substantial errors. The UEDGE potential has a shallow valley on the large-R side of the X-point, for which there is weak evidence in the experimental data (the 150 V contour at $z \approx -1.18$ m).

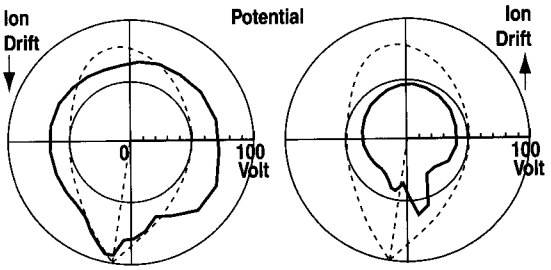

Fig. 8 Potential Φ versus poloidal angle, just inside the separatrix, for both directions of B_T. Dashed separatrix shape is added for reference.

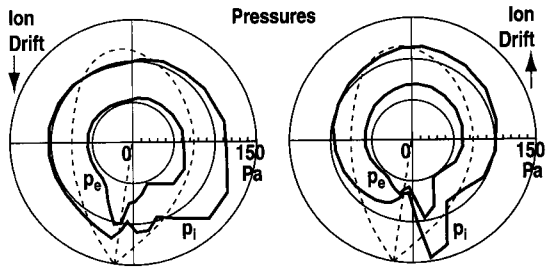

Fig. 9 Pressures p_e and p_i, as in Fig. 8.

Figure 8 shows the UEDGE-calculated potential Φ just inside the separatrix ($\psi_n = 0.9975$) for both B_T directions as a function of polar angle. The separatrix outline is shown to help the reader relate poloidal nonuniformities with geometric features. The UEDGE peak-to-peak variation, $\approx$ 30 V, is much smaller than measured difference between X-point and upstream. The UEDGE potential for standard B_T peaks at the X-point, but with reversed B_T there is only a small X-point peak, and the main peak is somewhat upstream. The corresponding calculated p_e on the same magnetic surface, Fig. 9, follow the Φ nonuniformity closely, because T_e is nearly uniform. Figure 9 also shows ion pressures, p_i, which are relatively lower at the X-point than p_e, because T_i decreases to about 50 eV near the X-point, from about 90 eV upstream on this surface.

Calculated total pressures, p, are shown in Fig. 10. The poloidal gradients of total pressure are surprising. Still more surprising, UEDGE-calculated parallel velocities are small, in that the divergence of the inertial tensor is much less than ∇p. Instead, Fig. 10 shows that most of $-\nabla_\parallel p$ is balanced by the gradient of the parallel viscous stress,

$$\pi_{i\parallel} = -(4/9)p_i\tau_{\perp\leftrightarrow\parallel}dv_\parallel/ds_\parallel \equiv -\eta_\parallel dv_\parallel/ds_\parallel \qquad (2)$$

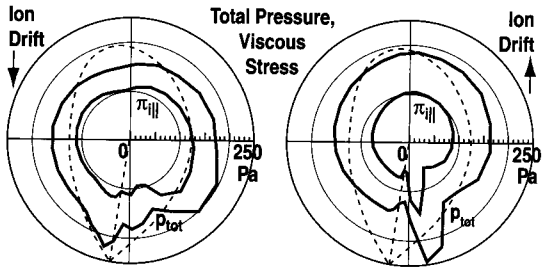

Fig. 10 Total pressure and parallel viscous stress as in Fig. 8. An arbitrary constant is added to $\pi_{i\|}$ for plotting convenience.

Here $\tau_{\perp\leftrightarrow\|}$ is the collisional relaxation time between ion parallel and perpendicular pressures [21,6], and $\tau_{\perp\leftrightarrow\|} \approx 2.5\tau_i$, where τ_i is the usual ion collision time [17]. The parallel viscous force, $f_{visc\|} = -\nabla_\| \pi_{i\|}$, opposes velocity derivatives. Since $\eta_\| \sim T_i^{5/2}$, a flux limit factor was used in the UEDGE calculations to limit $|\pi_{i\|}|$ to $< 0.5\ p_i$, in order to avoid unphysically large viscosity, but the numerical solutions were insensitive to the choice of flux limit (tested between 0.1 p_i and 1.0 p_i). The boundary layer is sufficiently collisional to justify this viscosity model.

According to the UEDGE modeling, the poloidal pressure nonuniformities arise where the parallel viscous force sufficiently impedes the Pfirsch-Schlüter ion return flow of the ∇B drift. For example, while ions drift vertically in the non-uniform B_T field toward the X-point, other ions return along B to the top of the plasma, and re-supply the ∇B drift. Due to the weak near-X poloidal B, the return flow divides between the inner (small R) and outer (large R) return options. This establishes $dv_\|/ds_\|$ in the X-region. If η is large, the viscous force exceeds the ion inertia, and the parallel gradient of the total pressure grows against the viscous force. Quasineutrality couples p_e and p_i through n_e, and the electron nonuniformities then generate the potential cells.

The potential peak at about 45° below the equator in Fig. 8 (for standard B_T) and valley (for reversed B_T) at about the same location is a robust feature of the low power UEDGE modeling with self-consistent drifts. These are stationary structures, and here, too, parallel viscosity balances most of the pressure gradient. We do not understand at present why these potential cells form. We conjecture that they are saturated instabilities. Experimental evidence for a stationary electric potential cell was found at the edge of the TEXTOR tokamak [22]. We conjecture that multiple potential cells and their associated cross-separatrix transport might be a common, perhaps ubiquitous, feature of low confinement behavior.

Although not shown here, the UEDGE toroidal rotation frequency, Ω, is very nonuniform near the separatrix, even changing sign around the poloidal circumference. We conjecture that the transition from L- to H-mode requires formation of a more poloidally-uniform boundary layer, one that permits a neoclassical-like uniform Ω and does not have the large cross-separatrix transport associated with electric potential cells. Poloidal homogenization was a feature of electrode-driven L- to H-transitions in the CCT limiter tokamak [23].

5. Conclusion

An electric potential hill and an associated electron pressure hill are measured at the divertor X-point in L-mode plasmas in DIII-D. The potential hill drives an $\boldsymbol{E}\times\boldsymbol{B}_T$ circulation about the X-point (potential cell), thereby exchanging plasma between closed and open magnetic surfaces at rates that can be comparable to the total cross-separatrix transport. Modeling by the 2D edge transport code UEDGE with ∇B and $\boldsymbol{E}\times\boldsymbol{B}$ drifts reproduces many of the observations. The code identifies parallel (to $\boldsymbol{B}$) viscous stress acting on the Pfirsch-Schlüter ion return flow of the ∇B drift as the origin of the pressure nonuniformity that generates potential cells in the boundary layer near the magnetic separatrix. The code also shows examples where small perturbations generate additional potential cells.

Acknowledgement

The authors acknowledge helpful discussion and contributions from D.R. Baker, K.H. Burrell, C.J. Lasnier, A.W. Leonard, R. Bulner, and T.S. Taylor. This work was supported by the U.S. Department of Energy under Contracts DE-AC03-99ER54463, DE-AC04-94AL85000, and Grant No. DE-FG03-95ER54294.

References

[1] F.L. Hinton and Y-B Kim, Nucl. Fusion **34**, 899 (1994).

[2] T.D. Rognlien *et al.*, J. Nucl. Mater. **196-198**, 347 (1992).

[3] G.R. Smith *et al.*, J. Nucl. Mater. **220-222**, 1024 (1995).

[4] T.D. Rognlien *et al.*, J. Nucl. Mater. **266-269**, 654 (1999).

[5] T.D. Rognlien *et al.*, Phys. Plasmas **6**, 1851 (1999).

[6] T.D. Rognlien *et al.*, Czechoslovak J. Phys. **48**,

Suppl. S2, 201 (1998).
[7] J.A. Boedo *et al.*, Phys. Plasmas **7**, 1075 (2000).
[8] J.C. Luxon and L.G. Davis, Fusion Technol. **8**, 441 (1985).
[9] M.J. Schaffer *et al.*, J. Nucl. Mater. **290-293**, 530 (2001).
[10] M.J. Schaffer *et al.*, Phys. Plasmas **8**, 2118 (2001).
[11] J.G. Watkins *et al.*, Rev. Sci. Instrum. **68**, 373 (1997).
[12] J.G. Watkins *et al.*, Rev. Sci. Instrum. **63**, 4728 (1992).
[13] T.N. Carlstrom *et al.*, Rev. Sci. Instrum. **68**, 1195 (1997).
[14] T.N. Carlstrom *et al.*, Rev. Sci. Instrum. **63**, 4901 (1992).
[15] P. Gohil *et al.*, Proc. of 14th Symp. on Fusion Engineering, San Diego, California, 1992, Vol. 2 (IEEE, New York, 1993) p. 1199.
[16] L.L. Lao *et al.*, Nucl. Fusion **25**, 1161 (1985).
[17] S.I. Braginskii, in *Reviews of Plasma Physics*, M.A. Leontovich, ed. (Consultants Bureau, New York, 1965) Vol. I, p. 205.
[18] R.J. Colchin *et al.*, Nucl. Fusion **40**, 175 (2000).
[19] M.A. Mahdavi *et al.*, J. Nucl. Mater. **176-177**, 32 (1990).
[20] B.A. Carreras *et al.*, Phys. Plasmas **3**, 4106 (1996).
[21] E. Zawaideh *et al.*, Phys. Fluids **29**, 463 (1986).
[22] J. Boedo *et al.*, Europhysics Conference Abstracts **19C**, Part 1, I-293 (1995).
[23] G.R. Tynan *et al.*, Plasma Phys. Control. Fusion, 1301 (1996).